Article

Analysis of the Charge Density Variation Caused by the Physical Properties of the Electrodes of Lithium-Ion Batteries

Xin Lu [1] and Ning Chen [2,*]

1   School of Automotive Engineering, Changshu Institute of Technology, Changshu 215500, China
2   Department of Mechanical and Electronic Engineering, Nanjing Forestry University, Nanjing 210037, China
*   Correspondence: chenning@njfu.com.cn

Abstract: The detection and characterization of electrode performance is a key problem of lithium-ion batteries. The physical properties of the electrodes affect the charge density during the life of a battery. The charge density is difficult to monitor because of the complexity of the charge distribution. In this paper, a visualized fractional derivative order (FDO) is used to characterize the charge distribution and to reveal variations in the charge density associated with the physical properties of the electrode. Instantaneous discharge datasets collected at different aging stages of batteries are used to identify the FDO in the fractional derivative model. The results show that the FDO has a strong correspondence with the charge density. As the charge density decreases, the charge mobility gradually increases due to changes in the charge distribution. Moreover, this paper finds that the capacity recovery effect is closely related to the mutation of the charge density and uses the FDO to explain the charge accumulation at the sharp edges of the electrodes. The analysis of the charge density variation caused by the physical properties of the electrodes provides guidance for the detection of the electrode performance and the design of the electrode microstructure.

Keywords: fractal distribution; fractional derivative model; charge density; electrode performance

1. Introduction

Lithium-ion batteries play a vital role in the functional integrity of entire systems and the ability to properly perform operational tasks [1,2]. The performance of batteries is closely related to the charge density on the electrodes [3–5]. The charge density changes with the remaining useful life of the battery due to changes in the physical properties of the electrodes [6,7]. Research on the charge density of electrodes can reveal the dynamic behavior inside the battery during the whole life cycle [8,9]. If the mechanism governing changes in the charge density can be monitored, the operating conditions of electric vehicles can be adjusted according to their actual operation, and the degradation rate of batteries can be effectively reduced. The study on the charge density variation of the electrodes can be used to detect the performance of the electrodes and provide guidance for the design of the electrode microstructure. In addition, the charge density of the electrodes affects the state of charge (SOC), aging, and capacity of the lithium-ion battery. Studying the charge density of the electrodes is of great significance to the SOC estimation, life estimation, and capacity estimation of batteries.

The electrochemical test method is the main means to study the kinetics and interface structure of electrodes [10–12]. The electrochemical model can reflect the internal dynamic behavior of the battery by analyzing the relationship between the macroscopic data outside the battery and the activity of the internal microscopic particles [13–15]. Cyclic voltammetry is commonly used to analyze the nature, mechanism, and kinetic parameters of electrode reactions [16–18]. Cyclic voltammetry clearly reveals the formation mechanism of the solid electrolyte interface (SEI) film. Constant potential intermittent titration and constant current intermittent titration are commonly used methods for determining the diffusion

coefficient of electrode materials [19–25]. Electrochemical impedance spectroscopy (EIS) is usually used to detect the influencing factors (ionic conductivity, ion diffusion, charge transfer, charge absorption, passivation film, etc.) of electrode performance. This method uses the measured impedance spectrum to study the electrode system, which can obtain more kinetic and structure information of the electrode interface than other conventional methods [26–30].

The equivalent circuit model is also frequently used to analyze the dynamic effects of batteries because it is accurate and concise. With the rise of fractional calculus theory, the fractional-order modeling method is introduced into the equivalent circuit model. Compared with the integer-order model, the dynamic characteristics of the lithium-ion battery described by the fractional-order model are more complete, and the state estimation of the lithium-ion battery based on the fractional-order model is more accurate [31–34]. M. Yu et al. [35] built a fractional-order equivalent circuit model based on electrochemical testing methods and used an iterative learning algorithm to optimize the parameters in the model. Y. Jia et al. [36] established a fractional-order model considering the electrolyte-phase diffusion of the battery and designed a new method to identify the system parameters. L. Zhang et al. [37] proposed a multi-domain parameter identification method based on a fractional-order model and applied an intelligent optimization algorithm to identify the parameters of the model.

The charge distribution on the porous fractal electrodes is difficult to characterize clearly. The charge on the porous electrode interacts with its adjacent charges. The conventional test method for detecting the charge density interferes with the interaction between charges, thereby disrupting the original charge distribution on the electrode. The charge distribution on the electrodes is not visually evident and is difficult to monitor directly in the process of dynamic charging and discharging.

The porous electrode exhibits self-similarity on the microscopic scale of the material, which exhibits a fractal dimension in the spatial dimension [38]. The charges of the same symbol on the electrode have a mutually exclusive effect, and the distribution of charges needs to satisfy the principle of minimum potential energy. Therefore, the charge distribution on the porous electrodes has fractal characteristics. A fractional derivative order (FDO) in the fractional derivative model of batteries can characterize the fractal distribution of the charges. Due to the change in the physical properties of electrodes during battery aging, the charge density of the electrodes gradually changes throughout the life cycle of the battery. The variation in the charge density causes a change in the fractal distribution of the charges. Therefore, the FDO characterizing the fractal distribution of charges changes with the remaining life of the battery.

The FDO is used in this paper to characterize the changes in the charge density. A fractional-order differential equation is established to simulate the charge distribution of the electrodes. Then, the instantaneous discharge datasets of batteries at different states of charge (SOCs) and cycle numbers are collected. Based on the optimization method, the FDO is identified using the collected current–voltage signal. The results show that there is a correspondence between the FDO and the charge density. As the charge density decreases, the charge mobility gradually increases due to changes in the physical properties of the electrodes, and the corresponding FDO increases. The FDO can be used as an indicator of the charge density and can be used to characterize the charge distribution, which cannot be directly detected. Finally, the FDO is used to explain the capacity of recovery phenomenon caused by the mutation of the charge density. The contribution of this paper is summarized as follows:

- The monitoring method for the charge density is a non-destructive testing method. The amount of data collected during the instantaneous discharge is small, and the battery does not need to be fully discharged. The proposed method is a fast and effective monitoring method, which is of great significance for battery performance detection in actual operation.

- The fractional derivative model is used to characterize the fractal distribution of the charges, and the FDO is used to reveal changes in the charge density.
- This paper explains the capacity recovery phenomenon from the perspective of the physical properties of electrodes.
- The study on the charge density variation of the electrode provides guidance for the detection of electrode performance and the design of electrode microstructure.

The remainder of this paper is organized as follows: In Section 2, the charge distribution of electrodes is studied. In Section 3, the battery model is built. In Section 4, the battery tests are performed. The FDO is identified in Section 5. Section 6 reveals the capacity recovery of the batteries. The conclusion is given in Section 7.

2. Charge Distribution on the Porous Electrodes

When a battery in the stationary state is exposed to an initial instantaneous drawn current, the lithium ions decomposed from the lithium–carbon interlayer compound dissociate into the solid electrolyte. Subsequently, the lithium ions pass through the separator to reach the surface of the cathode [39]. At the same time that lithium ions begin to move freely, the electrons pass from the anode to the cathode as driven by the external load. The movement of electrons causes charge to accumulate on the electrodes. The accumulation of charge causes the potential of the electrode to deviate from the initial equilibrium state [40–42]. On the other hand, the electrode reaction absorbs the charge accumulated on the electrode, causing the potential of the electrode to return to equilibrium. The electrode reaction includes the ion transport, ion diffusion at the interface of electrode, ion migration in the solid electrolyte membrane of the electrode, electrochemical reactions, ion diffusion in the solid phase, etc. [43,44].

Figure 1 shows the electric potential difference between the electrodes when the battery is discharged by an initial instantaneous load current. The battery has been left to stand for a while before the discharge test to stabilize the internal state. The current is loaded from time T1 to time T2 in Figure 1. The duration of the instantaneous discharge of the battery is short, and the complicated interfacial reaction between the electrode and the electrolyte has a hysteresis effect. In the instantaneous discharge process of the battery, the dynamical effects mainly depend on the charge accumulation at the electrodes, whereas the complex reaction between the electrodes and electrolyte interface accounts for a small proportion. This paper focuses on the accumulation phenomenon on the electrode and omits discussion of the electrode reaction.
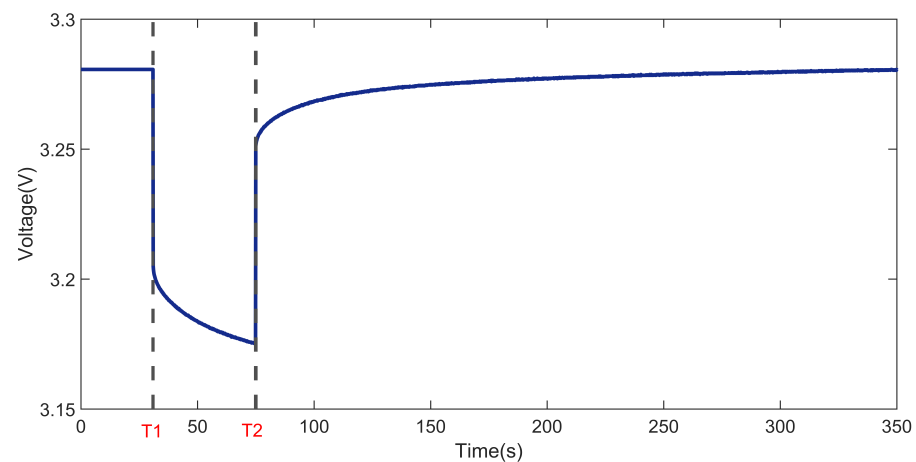

Figure 1. Potential difference between electrodes when the battery is loaded with an initial instantaneous current.

The porous electrode exhibits the property of self-similarity on the microscopic scale of the material, which exhibits a fractal dimension in space. The charges are arranged in a fractal morphology on the porous electrode. Therefore, the charge accumulation on the

porous electrode cannot be appropriately characterized by an ideal pure capacitor showing integer-order characteristics. A fractional capacitor can characterize the fractal distribution of the charges on the porous electrode. The impedance expression of the fractional capacitor can be expressed in the following form [45]:

$$Z(jw) = \frac{1}{C_f(jw)^\alpha} \tag{1}$$

where C_f ($C_f \in R$) is the coefficient of the fractional capacitor and α ($0 < \alpha < 1$) is the FDO. According to the characteristics of the fractional derivative definition, when the FDO is equal to 0, the fractional capacitor represents a resistor. When the FDO is equal to 1, the fractional capacitor represents an ideal pure capacitor [46–48].

In the life cycle of a battery, the fractal distribution of the charges on a porous electrode can be divided into two forms from the perspective of physical properties: the charge distributions at high density and those at low density. The fractal distribution of the charges can be approximately simulated as shown in Figure 2. Figure 2a shows the charge distribution at a high charge density, whereas Figure 2b shows the charge distribution at a low charge density.
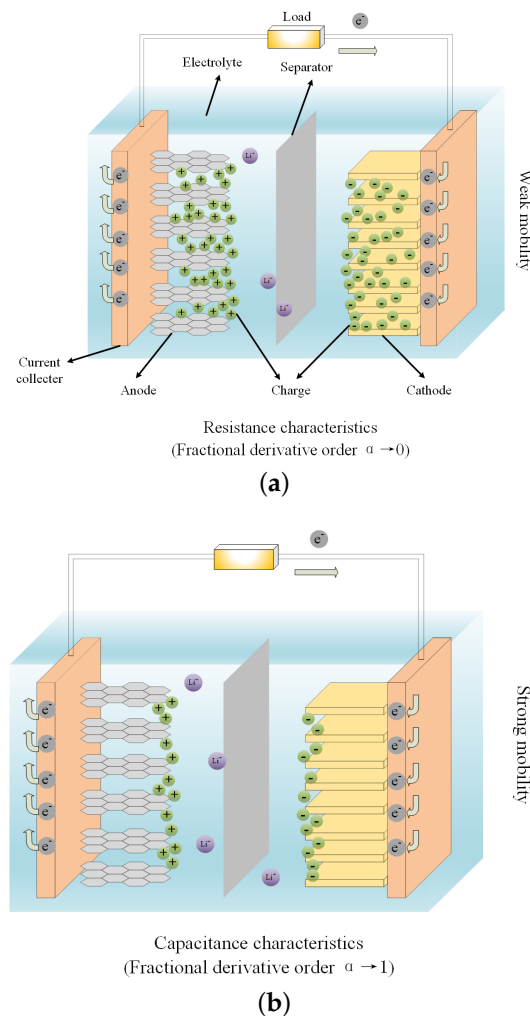

Figure 2. Fractal distribution of the charges on the porous electrodes: (**a**) high charge density; (**b**) low charge density.

When the charge density on the porous electrode is large, charge carriers partially intrude into the interior of the porous electrode due to the mutual repulsion of the same−sign

electric charges. The flow of charge intruding into the porous electrode is hindered by the adjacent charge, and thus, the overall mobility of the charge at a high charge density is poor. As a result, when the charge density is large, the electrode exhibit resistance characteristics, and the fractional capacitor characterizing the fractal distribution of charges converts into a resistor. More specifically, when the charge density is large, the FDO of the fractional capacitor tends towards 0.

Conversely, when the charge density on the electrode is small, the charges are mainly distributed on the surface of the electrodes. The flow resistance of the charges is reduced, and the charges on the electrodes exhibit strong mobility. At this moment, the arrangement of charges on the electrodes is similar to that of a pure capacitor. Therefore, when the charge density of the electrode is very small, the resistance characteristics of the electrode are weakened, and its capacitance characteristics are enhanced. As the charge density decreases, the fractional capacitor characterizing the charge distribution converts into a pure capacitor, and its corresponding FDO converges towards 1.

The charge distributions at high charge density and low charge density correspond to two different physical properties of the electrode. During the life cycle of a battery, the charge distribution changes between a high charge density state and a low charge density state due to changes in the physical properties of the electrode. Variations in the charge density change the fractal distribution of the charges, which in turn change the FDO of the fractional capacitor. Therefore, the change in the charge distribution can be characterized by the visualized FDO of the fractional capacitor, as shown in Equation (1). The FDO can be used as an indicator of the charge distribution to detect variations in the charge density. To reveal the specific changes in the charge density of the electrode over the whole life cycle of the battery, it is necessary to identify the FDO over the different aging stages of the batteries.

3. Battery Modeling

An equivalent circuit of the fractional derivative model of batteries can be used to simulate the output voltage of batteries under an instantaneous load current, which is shown in Figure 3. The equivalent circuit in Figure 3 is used to simulate the voltage response between time T1 and time T2 in Figure 1. In Figure 3, R_0 represents the ohmic impedance caused mainly by current collectors, the separator, and solid electrolytes; R_1 represents the depolarization effect, which is a simplification of complex electrode reactions; the fractional capacitor characterizes the charge accumulation phenomenon; I represents the instantaneous load current; U_{ocv} represents the open circuit voltage; U_f represents the voltage across the fractional capacitor; and U_t represents the output voltage. The continuous state equation and output equation of the equivalent circuit of the fractional derivative model of batteries can be written as [49–51]

$$\begin{cases} D^\alpha U_f = \dfrac{I}{C_f} - \dfrac{U_f}{R_1 C_f} \\ U_t = U_{ocv} - I R_0 - U_f \end{cases} \tag{2}$$

where D is the derivative operator.

Equation (2) can be converted to the form of state-space functions

$$\begin{cases} D^\alpha x = Ax + BI \\ y = Cx + DI \end{cases} \tag{3}$$

where $x = [U_f]$, $y = [U_t - U_{ocv}]$, $A = [-1/R_1 C_f]$, $B = [1/C_f]$, $C = [-1]$, and $D = [-R_0]$.

Equation (3) can be further discretized into the following forms:

$$\begin{cases} D^\alpha x_{k+1} = Ax_k + BI_k \\ y_k = Cx_k + DI_k \end{cases} \tag{4}$$

where $I_k \in R$ and $y_k \in R$ are the input and output of the system at time k, respectively.
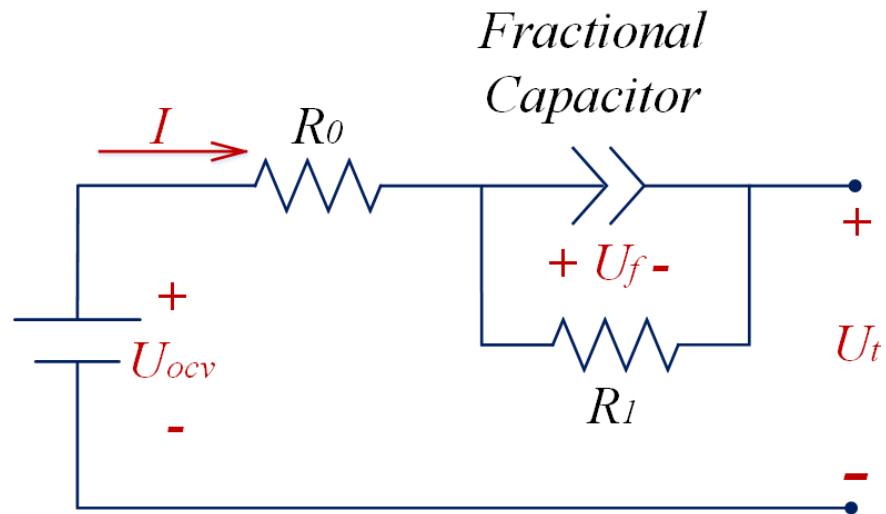

Figure 3. Equivalent circuit of the fractional derivative model of a battery under an instantaneous load current.

In the development of fractional calculus theory, a variety of fractional calculus definitions with different solutions have been presented [46,47,50,51]. The Grünwald–Letnikov fractional-order derivative definition is the most direct and commonly used numerical method for solving fractional calculus, and it is also applied to solve the solution of the proposed fractional discrete state space function of the potential difference between the electrodes. The Grünwald–Letnikov fractional derivative for state x at time step k is given as follows:

$$D^\alpha x_k = \frac{1}{T_s^\alpha} \sum_{j=0}^{k} (-1)^j \binom{\alpha}{j} x_{k-j}$$

$$\binom{\alpha}{j} = \begin{cases} 1 & j = 0 \\ \dfrac{\alpha(\alpha)\dots(\alpha-(j-1))}{j!} & j > 0 \end{cases} \tag{5}$$

where T_s is the calculating step length, j is the distance, and k is the requested sample amount.

According to the Grünwald–Letnikov fractional-order derivative definition, Equation (4) can be written as

$$
\begin{aligned}
D^\alpha x_{k+1} &= \frac{1}{T_s^\alpha} \sum_{j=0}^{k+1} (-1)^j \binom{\alpha}{j} x_{k+1-j} \\
&= \frac{1}{T_s^\alpha} (-1)^0 \binom{\alpha}{0} x_{k+1-0} + \frac{1}{T_s^\alpha} \sum_{j=1}^{k+1} (-1)^j \binom{\alpha}{j} x_{k+1-j} \\
&= \frac{1}{T_s^\alpha} \left[x_{k+1} + \sum_{j=1}^{k+1} (-1)^j \binom{\alpha}{j} x_{k+1-j} \right].
\end{aligned} \tag{6}
$$

Equation (6) can be further converted into the following form:

$$x_{k+1} = T_s^\alpha D^\alpha x_{k+1} - \sum_{j=1}^{k+1} (-1)^j \binom{\alpha}{j} x_{k+1-j}$$

$$= T_s^\alpha (A x_k + B I_k) - \sum_{j=1}^{k+1} (-1)^j \binom{\alpha}{j} x_{k+1-j}. \tag{7}$$

Finally, the output equation of the presented model can be discretized as

$$y_k = C x_k + D I_k \tag{8}$$

Equations (7) and (8) constitute the fractional discrete output equation and state equation of the battery model, respectively.

4. Experiment

To study the variation in the FDO in the life cycle of the batteries, a battery test platform is established to collect a battery-related dataset. First, an SOC test of the battery is performed, and the data of the instantaneous discharge are collected at different battery SOCs. Then, a battery aging test is carried out to collect a dataset of the instantaneous discharge properties at different cycle numbers of the batteries.

4.1. Test Platform

The battery test platform consists of a temperature chamber, a battery tester (Arbin Instruments, College Station, TX, USA), a signal control and measurement unit, a conversion unit, a computer, and lithium-ion ($LiNi_x Mn_y Co_z O_2$) batteries. The Arbin BT2000 tester collects the charge/discharge data of batteries at a fixed frequency and then stores the data on the computer through the conversion unit. The Arbin BT2000 test system has special monitoring software for the upper computer, which can realize complex programmable load control, arbitrary load power control, current control, etc. The measured data and calculated values can be displayed and stored dynamically in real time. The collected data mainly include the discharge current, capacity, terminal voltage, time interval, and temperature. The scheme of the test platform of lithium-ion batteries is shown in Figure 4.
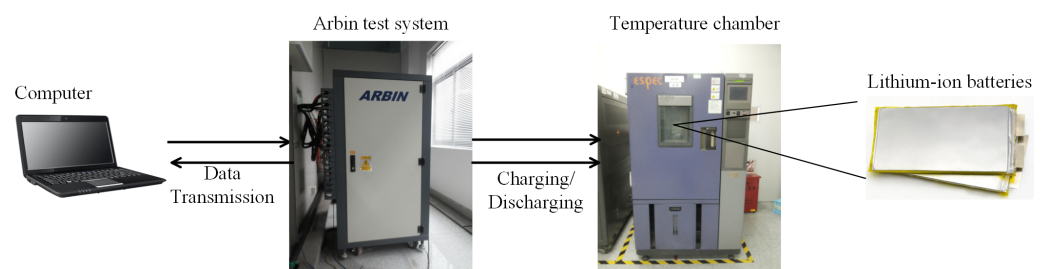
Figure 4. The scheme of the test platform of lithium-ion batteries.

Part of the appearance specifications of the lithium-ion battery to be tested are shown in Table 1.

Table 1. Part of the appearance specifications of the lithium-ion battery.

Battery	Nominal Capacity (Ah)	Discharge Cut-Off Voltage (V)	Charge Cut-Off Voltage (V)	Operating Temperature (°C)
$LiNi_x Mn_y Co_z O_2$	10	2.2	4.2	25

4.2. Battery SOC Test

To study the variation in the FDO for different SOCs, three lithium-ion batteries of the same specification, labelled Nos. 001, 002, and 003, are tested at a constant temperature (25 °C). The batteries are charged at a constant current (CC) of 0.5 C until the terminal voltage reaches the charge cut-off voltage. Then, the batteries are continuously charged at a constant-voltage (CV) mode until the charging current drops to 0.5 A, at which point the charging process is ended. Finally, the batteries are allowed to stand for 1 h. During the discharge process, the entire SOC of the battery is divided into 20 segments, and the batteries are discharged with the instantaneous current for every 5% of the SOC. The specific details of the discharge process of the SOC test are as follows:

1. The batteries are discharged with an initial instantaneous load current of 1 C for a duration of 45 s. The current is loaded from time T1 (31st s) to time T2 (75th s).
2. The applied load is cut off, and the batteries are left to stand for 5 min.
3. The batteries are discharged by a constant current of 0.5 C until the battery SOC drops by 5%.
4. The applied load is cut off, and the batteries are left to stand for 35 min.
5. Repeat steps 1, 2, 3, and 4 until the battery SOC is 0%, at which point the SOC test of the batteries is ended.

4.3. Aging Test

To study the variation in the FDO at different aging stages of batteries, battery Nos. 001, 002, and 003 are tested at a constant temperature (25 °C). The instantaneous discharge test is carried out at different charging/discharging cycles. The specific details of the aging test are as follows:

1. The batteries are charged at a constant current of 0.5 C until the voltage reaches the charge cut-off voltage. Then, the batteries are continuously charged in CV mode until the charging current drops to 0.5 A. Subsequently, the batteries are allowed to stand for 1 h. The charging capacity of the battery is recorded.
2. The batteries are discharged with an initial instantaneous current of 1 C for a duration of 45 s. The current is loaded from time T1 (31st s) to time T2 (75th s).
3. The applied load is cut off, and the batteries are left to stand for 5 min.
4. The batteries are discharged with a constant current of 0.5 C until the SOC drops to 0%.
5. The applied load is cut off, and the batteries are left to stand for 35 min.
6. Fifty charge/discharge cycles of batteries are performed in the constant current–constant voltage (CC-CV) mode. The batteries are first charged to the charge cut-off voltage by the CC-CV mode. Then, the batteries are discharged to the discharge cut-off voltage by the CC mode of 0.5 C and continue to be discharged by the CV mode until the current is less than 0.5 A.
7. Repeat all the above steps until the capacity drops by 30%, at which point the aging test is ended.

Figure 5 shows the output voltage of instantaneous discharge of battery No. 001 at different SOCs and different cycle numbers. The sampling frequency of the battery tester is 10 Hz, and the curves shown in Figure 5 are interpolated. The instantaneous current is loaded from time T1 to time T2 in Figure 5. The dataset acquired during the instantaneous discharge at each SOC and cycle number is used to identify the FDO.

The voltage response at 0% SOC exhibits a high nonlinearity and is therefore excluded from the research. In the battery aging test, the total number of charge/discharge cycles of the batteries is 825.
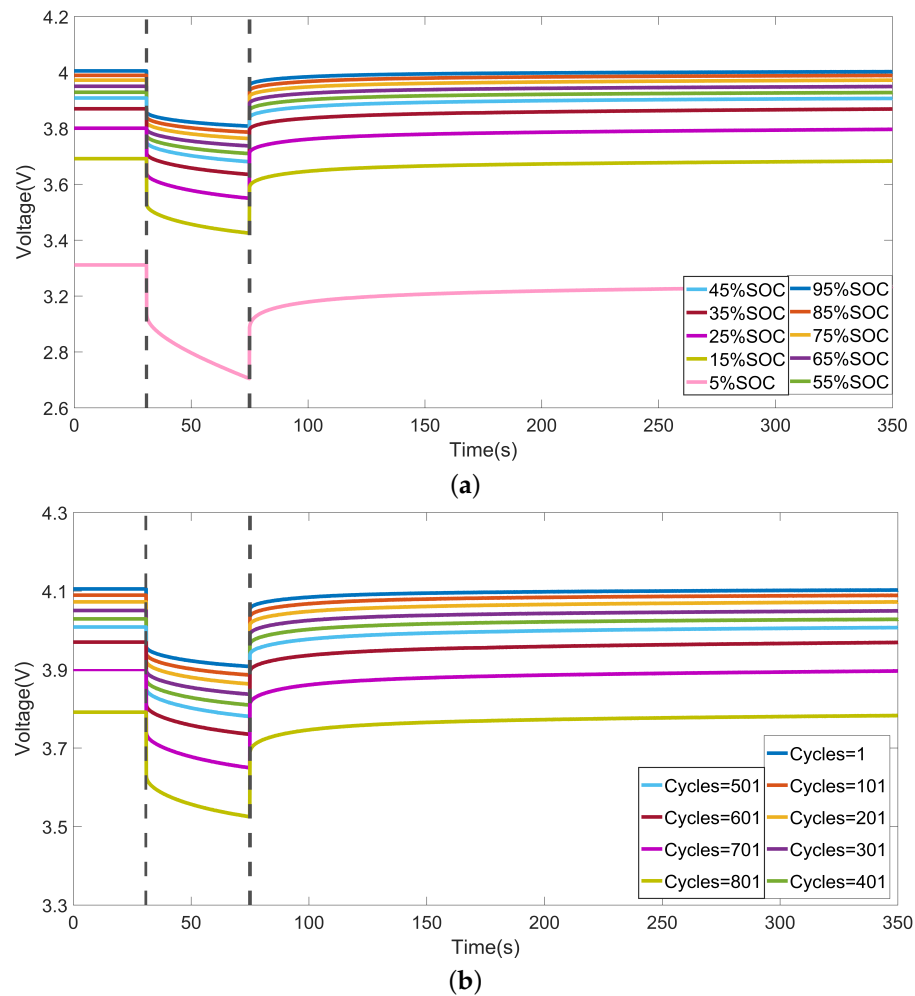
Figure 5. Output voltage of the instantaneous discharge of battery No. 001: (**a**) at different SOCs; (**b**) at different cycle numbers.

5. Identification of the FDO

The FDO is identified using the least squares method. Subsequently, the variations in the FDO at different SOCs and cycle numbers are analyzed.

5.1. Identification Method

The least squares method is a commonly used mathematical optimization method, which can obtain the optimal matching of a function of the collected dataset by minimizing the sum of squared errors [52,53]. The least squares method is suitable for static, dynamic, linear, and nonlinear systems and is also adopted in this section. The battery in the discharge state is considered a dynamic system. The instantaneous current is used as the input of the system, and the estimated voltage is seen as the output of the system. The error between the estimated voltage and the measured voltage is used as an indicator for evaluating the accuracy of the model. The purpose of identification is to search for the optimal variable FDO in the fractional-order differential equation. The optimization criteria for the fractional-order differential equation can be expressed as [42,54]

$$Fit = \min\left\{\sum_{k=T_0}^{T}[y_k - \widehat{y}_k]^2\right\} \tag{9}$$

where $\widehat{y}_k$ is the estimated output voltage and y_k is the measured output voltage at time k.

The resistance R_0 is calculated by the voltage drop at the initial time point of the discharge test. Different from other parameters in the fractional derivative model, the variation in the FDO in the fractional-order differential equation characterizes different dynamic behaviors of the electrodes. In the identification process of the fractional derivative model, it is not appropriate to identify the FDO together with other parameters. Hence, the FDO is individually identified by the least squares method. The coefficient C_f of the fractional capacitor is selected according to the characteristics of the tested battery and is used as a constant. The basic operation steps of the least squares method are as follows:

- The boundary values of the FDO α and resistance R_1 are set, and a series of random FDOs and resistances are generated from the uniform distribution. The initial values of α and R_1 are selected at 0.5.
- The values of the coefficient C_f and the ohmic resistance R_0 are set.
- The current series ($I = [I_k | k = 1, 2, \ldots, n]$) of the instantaneous discharge collected by the experimental platform are substituted into the fractional-order differential equation to calculate the estimated voltage ($\hat{y} = [\hat{y}_k | k = 1, 2, \ldots, n]$).
- The measured voltage ($y = [y_k | k = 1, 2, \ldots, n]$) and estimated voltage between time T1 and time T2 are fitted by the optimization algorithm.
- The objective function is calculated according to the error between the measured voltage and the estimated voltage.
- The objective function is optimized iteratively to determine the optimal FDO α and resistance R_1 so that the fitting error reaches the minimum value.

The instantaneous discharge datasets at different SOCs and charge/discharge cycles are used to identify the corresponding FDO.

5.2. Identification Results

The fitting result of the output voltage under the instantaneous current is shown in Figure 6. Because the amount of collected data during the instantaneous discharge process is small and the fractional derivative model is simplified, the entire identification process consumes only a short time and requires minimal computation.
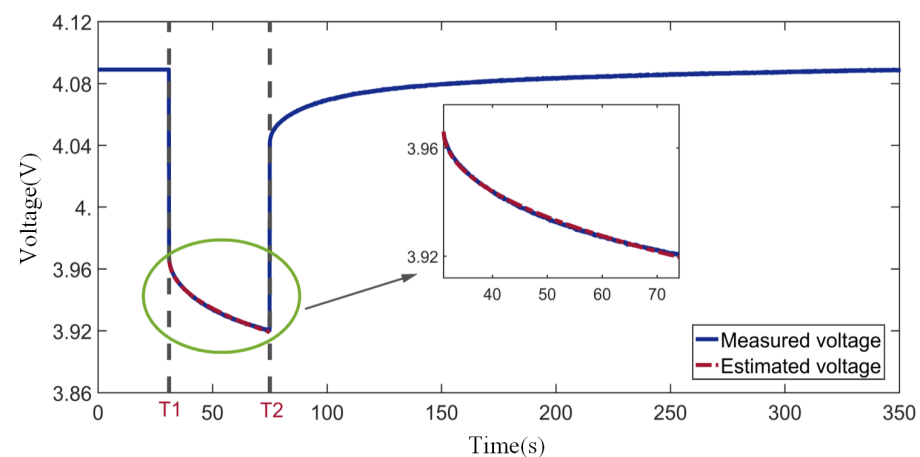

Figure 6. Fitting result of the output voltage of instantaneous discharge at the first cycle number (battery No. 001).

Table 2 shows the resistance R_0 and R_1 at different SOCs, and Table 3 shows the resistance R_0 and R_1 at different cycle numbers.

Table 2. Resistance R_0 and resistance R_1 at different SOCs.

SOC/%	10	20	30	40	50	60	70	80	90	100
R_0 (mΩ)	16.39	16.10	15.94	15.68	15.49	15.33	15.13	15.00	14.75	14.32
R_1 (mΩ)	1.38	1.37	1.37	1.37	1.35	1.35	1.34	1.32	1.32	1.31

Table 3. Resistance R_0 and resistance R_1 at different cycle numbers (100% SOC).

Cycle	0	100	200	300	400	500	600	700	800
R_0 (mΩ)	14.68	14.87	14.94	15.26	15.39	15.59	15.84	16.04	16.27
R_1 (mΩ)	1.31	1.33	1.33	1.34	1.35	1.35	1.35	1.37	1.37

The FDOs identified at different SOCs and at different cycle numbers are shown in Figure 7. Figure 7a shows the FDOs identified at different SOCs, and Figure 7b shows the FDOs identified at different cycle numbers. The coefficient C_f of the fractional capacitor is set to 1000.

(**a**)

(**b**)
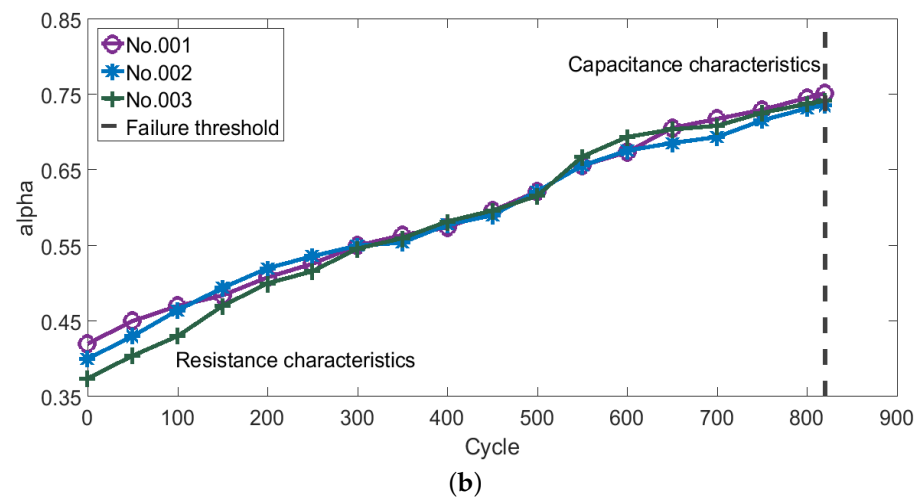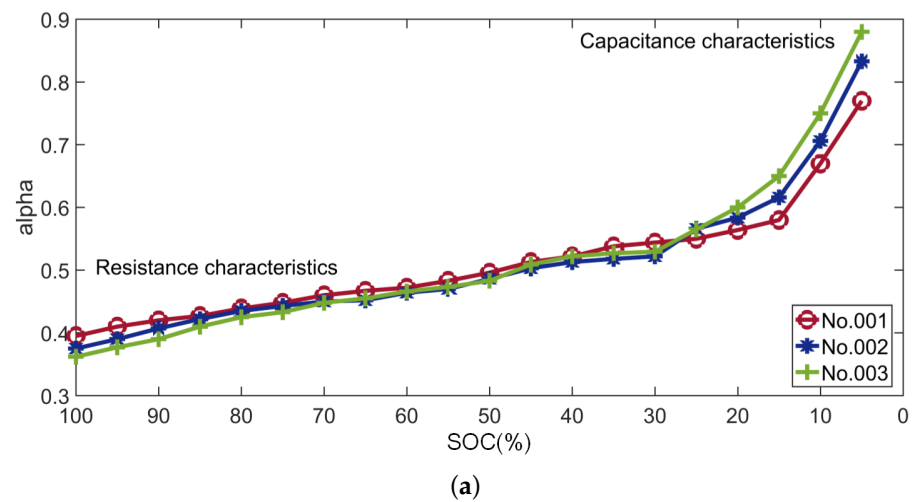
Figure 7. Identified FDO of the proposed battery model ($C_f = 1000$): (**a**) at different SOCs; (**b**) at different cycle numbers.

As seen in Figure 7a, the FDO of the battery model increases monotonically as the SOC decreases. The variation in the FDO characterizes the process of the electrode changing from resistive behavior to capacitive behavior and the process of changing from a high charge density state to a low charge density state. When the battery SOC is high, the charge density of the electrode is large, and the amount of charge entering the inside of the electrode is large. Therefore, the electrode exhibits resistive behavior, and its corresponding FDO tends towards 0. As the SOC drops from 100% to 15%, the FDO increases slowly. This phenomenon indicates that the resistive behavior component of the electrode is slowly decreasing, and the amount of the same-sign electric charge intruding into the electrode is gradually reduced. When the value of SOC is less than 15%, the slope of the SOC-FDO curve increases significantly. At this stage, the capacitive behavior of the electrode increases rapidly. At the end of the SOC test, the charge density of the electrode is small, and the charges are mainly distributed on the surface of the electrodes. Therefore, when the SOC is low, the FDO corresponding to the charge density on the electrode tends towards 1.

Figure 7b shows the variation in the FDO at different charge/discharge cycles of the tested batteries. It can be seen from Figure 7b that the FDO is also monotonically increasing with increasing cycle number, indicating the tendency for the electrode characteristics to change from resistive to capacitive over the whole life cycle.

At the beginning of the life cycle of batteries, the charge density of batteries is large, and the porous structure of electrodes is intact, which shows the strong fractal property. A part of the charge invades the inside of the electrode, and the flow resistance of this part of the charge is enhanced. The fresh battery exhibits resistive characteristics, and its corresponding FDO tends towards 0.

As the battery ages, the fractal structure of the electrode changes due to the variation in the dynamic behavior of the battery, and the charge on the porous electrodes rearranges at the next cycling time. Some areas of the electrode active materials are damaged and can no longer accept the insertion of active lithium ions as the battery ages [55–58]. The volume variation of each active particle is affected by adjacent active particles and inactive components. In the charge and discharge process, the process of lithium intercalation leads to the internal strain of particles, and some side reactions also cause strain in the particles, resulting in deformation of the electrode structure. Moreover, heat is generated when lithium ions are inserted into active materials, resulting in volume expansion of the active particles. The fracture of these particles reduces the particle size and hinders electrolyte deposition on the electrode surface [59]. All these aging phenomena result in variations in the porosity of the electrode, leading to variations in the fractal distribution of charges on the electrode.

In the cyclic aging test of batteries, there is a process from quantitative changes to qualitative changes for the electrode characteristics. When the battery ages to a certain extent, the surface of the electrode is broken down by the charges. At the end of the battery life cycle, the charge is mainly distributed on the surface of the electrode, and the mobility of the charge increases. Therefore, the identified FDO tends towards 1, and the electrode shows capacitive characteristics.

The FDO can be used to reveal the variation in the charge density on porous electrodes. The current magnitude and temperature during the aging test affect the value of the identified FDO. The effect of temperature and current on the identified FDO has been discussed in detail in our previous studies [42]. When the coefficient C_f of the fractional capacitor is set at different values, the correspondence between the FDO and the cycle number is shown in Table 4.

It is worth noting that the battery is continuously charged and discharged in the aging test, and the collection interval of the discharge test is relatively long. Therefore, the capacity recovery effect of the battery in this section is not obvious, and the corresponding FDO has no obvious fluctuation.

Table 4. Correspondence between the FDO and the cycle number (battery No. 001).

C_f	1500	1400	1300	1200	1100	1000	900	800	700	600	500	400
*Cycle*1	0.555	0.535	0.514	0.493	0.470	0.456	0.431	0.414	0.394	0.372	0.356	0.333
*Cycle*51	0.578	0.559	0.538	0.516	0.493	0.479	0.454	0.437	0.418	0.395	0.379	0.357
*Cycle*101	0.598	0.579	0.555	0.532	0.518	0.492	0.475	0.456	0.435	0.410	0.391	0.375
*Cycle*151	0.608	0.587	0.565	0.542	0.528	0.502	0.485	0.467	0.445	0.420	0.401	0.386
*Cycle*201	0.625	0.604	0.582	0.569	0.545	0.520	0.503	0.484	0.462	0.447	0.428	0.403
*Cycle*251	0.631	0.610	0.598	0.575	0.551	0.536	0.519	0.490	0.479	0.454	0.435	0.419
*Cycle*301	0.650	0.639	0.617	0.594	0.570	0.555	0.538	0.519	0.497	0.473	0.453	0.438
*Cycle*351	0.687	0.666	0.644	0.621	0.607	0.582	0.565	0.546	0.525	0.500	0.481	0.465
*Cycle*401	0.702	0.681	0.669	0.646	0.622	0.607	0.580	0.561	0.549	0.525	0.501	0.480
*Cycle*451	0.724	0.703	0.681	0.668	0.644	0.629	0.602	0.583	0.561	0.547	0.527	0.502
*Cycle*501	0.731	0.710	0.698	0.675	0.651	0.636	0.619	0.590	0.579	0.554	0.535	0.519
*Cycle*551	0.754	0.733	0.711	0.698	0.674	0.659	0.632	0.613	0.591	0.577	0.558	0.532
*Cycle*601	0.775	0.753	0.731	0.718	0.694	0.679	0.652	0.633	0.612	0.597	0.578	0.552
*Cycle*651	0.782	0.760	0.748	0.725	0.701	0.686	0.669	0.640	0.629	0.604	0.584	0.569
*Cycle*701	0.817	0.792	0.776	0.754	0.732	0.718	0.692	0.675	0.656	0.634	0.617	0.595
*Cycle*751	0.839	0.818	0.796	0.773	0.759	0.733	0.717	0.698	0.676	0.651	0.632	0.617
*Cycle*801	0.847	0.824	0.806	0.785	0.762	0.748	0.723	0.706	0.686	0.664	0.648	0.625
*Cycle*825	0.854	0.834	0.812	0.790	0.776	0.757	0.738	0.719	0.692	0.678	0.655	0.634

6. Mutation of the Charge Density on the Electrodes

During the aging process of batteries, their capacity decreases gradually with increasing cycle time. However, in actual operation, the capacity recovers several times during the battery life cycle. The specific performance is that the capacity measured one cycle after storage is significantly higher than the capacity measured in the last cycle. The capacity recovery phenomenon is more obvious in the early stage of battery degradation and can even be higher than the initially measured capacity of the battery.

The capacity recovery of batteries is closely related to the mutation of the charge density, and this mutation is mainly caused by changes in the physical properties of the electrode. During the degradation of a battery, the porous electrode fractures under the aging mechanism and fatigue induced by thermal stress, and this process splits the electrode into a large number of small fragments with sharp edges. Under the action of electric power, these small, sharp edges of the electrodes attract a large amount of residual charge in a short time. As a result, the charge density of the electrode rises instantaneously, and the battery capacity recovers at these moments.

Datasets of cyclic aging tests of lithium-ion batteries from the National Aeronautics and Space Administration (NASA) Ames Prognostics Center of Excellence are used to analyse the capacity recovery phenomenon of batteries [60]. That laboratory performed life degradation experiments on several groups of lithium-ion batteries under different conditions and obtained a large amount of high-quality experimental data. In this paper, a set of battery data (battery numbers 0005, 0006, and 0007) is selected to identify the corresponding FDO at different cycle numbers. The rated capacity of the NASA batteries is 2 Ah. Part of the test procedures for the NASA batteries is shown in Table 5.

Table 5. Partial test procedure of the NASA batteries.

Battery Number	Charge Current (A)	Discharge Current (A)	Temperature (°C)	Charge Cut-Off Voltage (V)	Discharge Cut-Off Voltage (V)
No. 0005	1.5	2.0	24	4.2	2.7
No. 0006	1.5	2.0	24	4.2	2.5
No. 0007	1.5	2.0	24	4.2	2.2

The lithium-ion batteries are fully charged in constant-current, constant-voltage mode, and then the batteries are discharged in constant-current mode until the batteries reach the cut-off voltage. The batteries are cyclically charged and discharged until the capacity reaches the fault threshold. The total number of charge/discharge cycles of the batteries is 168. The output voltage of constant discharge of the NASA lithium-ion battery is shown in Figure 8. The data of the initial instantaneous discharge of the NASA battery are used for the identification of the fractional derivative model, which is shown from time T1 to time T2 in Figure 8. Because the sampling frequency of the NASA batteries is relatively low, this paper obtains the intercept of the long discharge duration to obtain sufficient data, thus ensuring the effectiveness of the identification process.
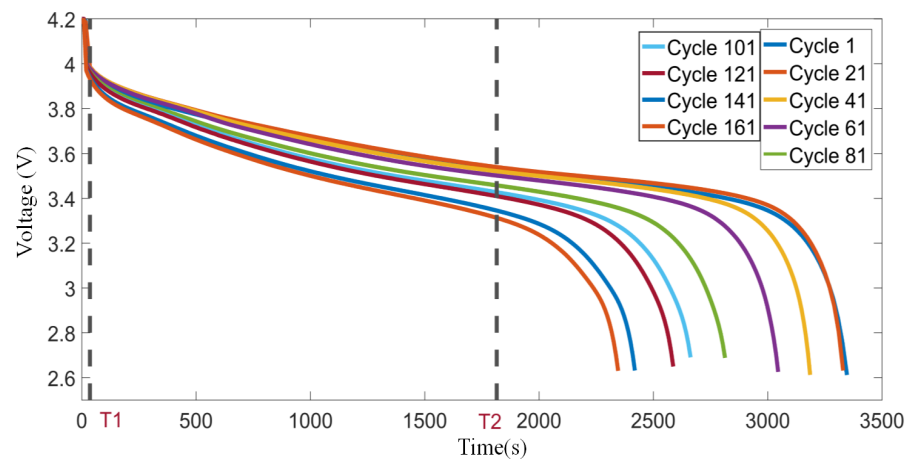

Figure 8. Output voltage of constant discharge of NASA battery No. 0005 at different cycle numbers.

Figure 9 shows the identified FDO and the capacity degradation curve of the NASA batteries. It is obvious from Figure 9 that the corresponding FDO suddenly drops at the moment of capacity recovery. The variation in the FDO indicates that the electrode exhibits resistive behavior at the point of capacity recovery. Due to the appearance of small, sharp edges, the charge density on the electrodes increases in a short time. The FDO as an indicator of the charge density change can well reflect the battery capacity recovery effect. Because the FDO is identified from the initial instantaneous discharge data of the battery, the FDO can be used to predict the possible capacity recovery effect. Furthermore, because the acquisition time of battery data is short and the identification of the least squares method is fast, the prediction method of this paper is easy to implement to monitor the electrode performance in real time.

In the instantaneous discharge process of the battery, the dynamical behavior mainly depends on the charge accumulation at the electrodes. The change in the charge density is primarily dependent on changes in the physical properties of the electrode. The FDO can be used to characterize the variations in the charge density, which cannot be directly detected. The method presented in this paper is a supplement to the conventional methods for monitoring the performance of electrodes. In the process of electrode manufacturing, if appropriate technologies (electrical discharge machining, laser processing, etc.) are used to create some artificial fractal cracks on the electrode, the charge density of the electrode can be improved and the damage caused by thermal stress can be reduced.
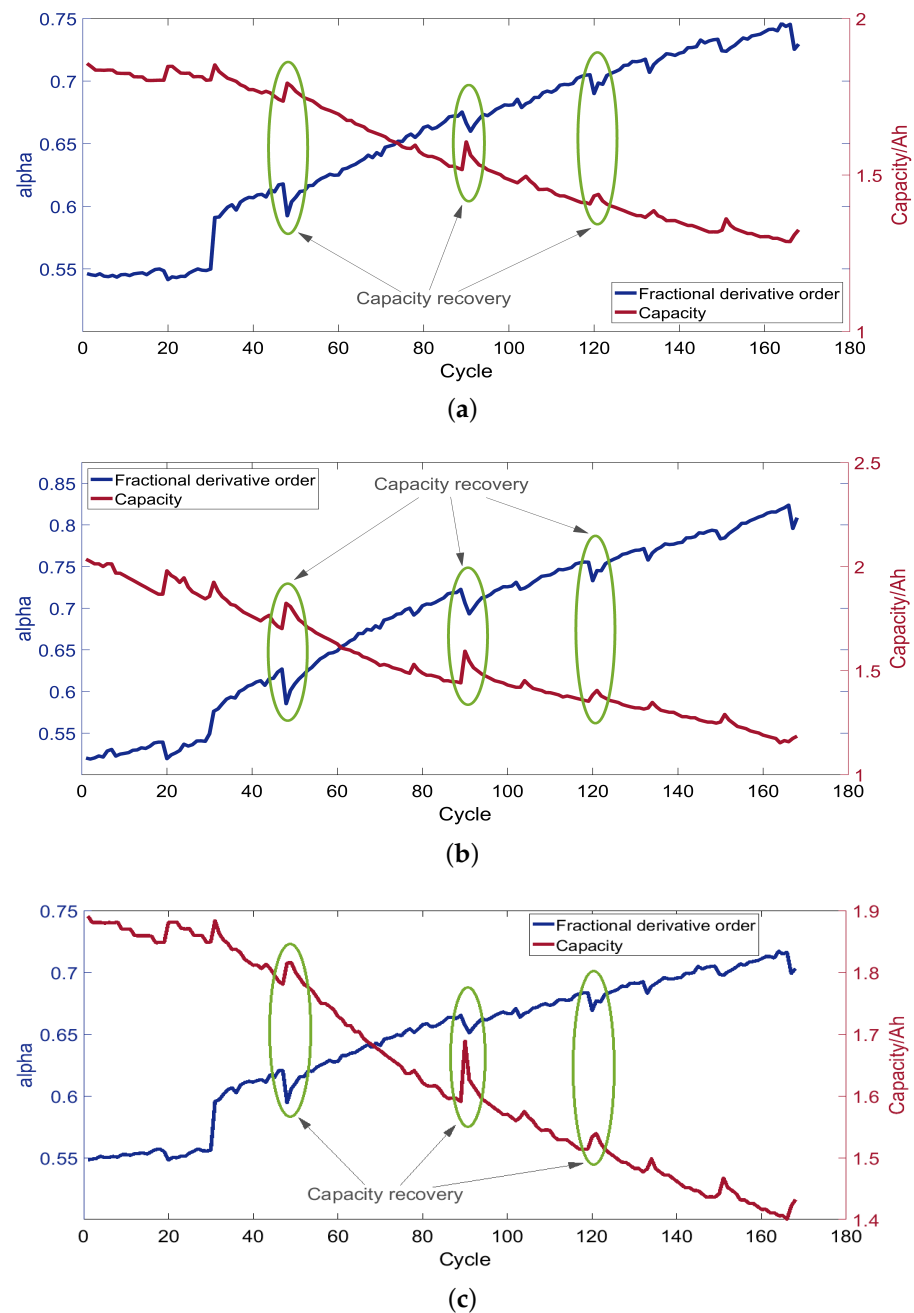
Figure 9. Identified FDO and the capacity degradation curve of the NASA18650 commercial lithium batteries: (**a**) battery 0005; (**b**) battery 0006; (**c**) battery 0007.

7. Conclusions

Because of the interaction of charge distribution on the electrodes, it is difficult to detect the changes in the charge density directly. In this paper, the FDO is used to characterize the fractal distribution of charge and to detect variations in the charge density. The Grünwald–Letnikov fractional order derivative definition is used to spatially discretize the fractional-order differential equation. The optimization method is used to identify the FDO at different SOCs and different aging stages. Changes in the FDO indicate that the charge mobility gradually increases as the charge density decreases. Finally, the FDO is used to explain the capacity recovery effect. The FDO can reveal changes in the charge density from the perspective of the physical properties of the electrode. This paper establishes a mathematical connection between the internal mechanism of the battery and the external measurable data. Monitoring the charge density with the FDO is a rapid and

non-destructive technique, which is easy to apply to dynamically monitor the performance of electrodes during the battery life cycle.

References

1. Vykhodtsev, A.V.; Jang, D.; Wang, Q.; Rosehart, W.; Zareipour, H. A review of modelling approaches to characterize lithium-ion battery energy storage systems in techno-economic analyses of power systems. *Renew. Sustain. Energy Rev.* **2022**, *166*, 112584. [CrossRef]
2. Ali, H.; Khan, H.A.; Pecht, M. Preprocessing of spent lithium-ion batteries for recycling: Need, methods, and trends. *Renew. Sustain. Energy Rev.* **2022**, *168*, 112809. [CrossRef]
3. Tahir, M.W.; Merten, C. Multi-scale thermal modeling, experimental validation, and thermal characterization of a high-power lithium-ion cell for automobile application. *Energy Convers. Manag.* **2022**, *258*, 115490. [CrossRef]
4. Nguyen, B.; Chazelle, S.; Cerbelaud, M.; Porcher, W.; Lestriez, B. Manufacturing of industry-relevant silicon negative composite electrodes for lithium ion-cells. *J. Power Sources* **2014**, *262*, 112. [CrossRef]
5. Wen, J.; Zhao, D.; Zhang, C. An overview of electricity powered vehicles: Lithium-ion battery energy storage density and energy conversion efficiency. *Renew. Energy* **2020**, *162*, 1629–1648. [CrossRef]
6. Gozdur, R.; Guzowski, B.; Dimitrova, Z.; Noury, A.; Mitukiewicz, G.; Batory, D. An energy balance evaluation in lithium-ion battery module under high temperature operation. *Energy Convers. Manag.* **2021**, *227*, 113565. [CrossRef]
7. Lu, L.; Han, X.; Li, J.; Hua, J.; Ouyang, M. A review on the key issues for lithium-ion battery management in electric vehicles. *J. Power Sources* **2013**, *226*, 272–288. [CrossRef]
8. Monaco, S.; Giorgio, F.D.; Col, L.D.; Riché, M.; Arbizzani, C.; Mastragostino, M. Electrochemical performance of $LiNi_{0.5}Mn_{1.5}O_4$ composite electrodes featuring carbons and reduced graphene oxide. *J. Power Sources* **2015**, *278*, 733–740. [CrossRef]
9. Scrosati, B.; Garche, J. Lithium batteries: Status, prospects and future. *J. Power Sources* **2010**, *195*, 2419–2430. [CrossRef]
10. Jiang, B.; Zhu, J.; Wang, X.; Wei, X.; Shang, W.; Dai, H. A comparative study of different features extracted from electrochemical impedance spectroscopy in state of health estimation for lithium-ion batteries. *Appl. Energy* **2022**, *322*, 119502. . [CrossRef]
11. Orazem, M.E.; Tribollet, B. An integrated approach to electrochemical impedance spectroscopy. *Electrochim. Acta* **2008**, *53*, 7360–7366.
12. Zhang, G.; Wei, X.; Zhu, J.; Chen, S.; Han, G.; Dai, H. Revealing the failure mechanisms of lithium-ion batteries during dynamic overcharge. *J. Power Sources* **2022**, *543*, 231867. [CrossRef]
13. Su, X.; Sun, B.; Wang, J.; Zhang, W.; Ma, S.; He, X.; Ruan, H. Fast capacity estimation for lithium-ion battery based on online identification of low-frequency electrochemical impedance spectroscopy and Gaussian process regression. *Appl. Energy* **2022**, *322*, 119516. [CrossRef]
14. Schmidt, J.P.; Chrobak, T.; Ender, M.; Illig, J.; Klotz, D.; Ivers-Tiffée, E. Studies on $LiFePO_4$ as cathode material using impedance spectroscopy. *J. Power Sources* **2011**, *196*, 5342–5348. [CrossRef]
15. Kurzweil, P.; Fischle, H.J. A new monitoring method for electrochemical aggregates by impedance spectroscopy. *J. Power Sources* **2004**, *127*, 331–340. [CrossRef]
16. Kim, S.; Choi, Y.Y.; Choi, J.I. Impedance-based capacity estimation for lithium-ion batteries using generative adversarial network. *Appl. Energy* **2022**, *308*, 118317. [CrossRef]
17. Tezyk, V.; Rossignol, C.; Sergent, N.; Djurado, E.; Laurencin, J.; Siebert, E. Cyclic voltammetry and high-frequency series resistance of $La_{0.6}Sr_{0.4}Co_{0.2}Fe_{0.8}O_{3-\delta}$ electrode deposited on GDC: Effect of the electrode microstructure and the oxygen partial pressure. *Electrochim. Acta* **2019**, *304*, 312–322. [CrossRef]
18. Pell, W.G.; Conway, B.E. Analysis of power limitations at porous supercapacitor electrodes under cyclic voltammetry modulation and dc charge. *J. Power Sources* **2001**, *96*, 57–67. [CrossRef]
19. Zhu, X.; Hallemans, N.; Wouters, B.; Claessens, R.; Lataire, J.; Hubin, A. Operando odd random phase electrochemical impedance spectroscopy as a promising tool for monitoring lithium-ion batteries during fast charging. *J. Power Sources* **2022**, *544*, 231852. [CrossRef]
20. Mao, Z.; Farkhondeh, M.; Pritzker, M.; Fowler, M.; Chen, Z. Dynamics of a Blended Lithium-Ion Battery Electrode during Galvanostatic Intermittent Titration Technique. *Electrochim. Acta* **2016**, *222*, 1741–1750. [CrossRef]
21. Chen, Y.; Wang, L.; Anwar, T.; Zhao, Y.; Piao, N.; He, X.; Zhu, Q. Application of Galvanostatic Intermittent Titration Technique to Investigate Phase Transformation of $LiFePO_4$ Nanoparticles. *Electrochim. Acta* **2017**, *241*, 132–140. [CrossRef]

22. Li, J.; Yang, F.; Xiao, X.; Verbrugge, M.W.; Cheng, Y.T. Potentiostatic intermittent titration technique (PITT) for spherical particles with finite interfacial kinetics. *Electrochim. Acta* **2012**, *75*, 56–61. [CrossRef]

23. Churikov, A.; Ivanishchev, A.; Ivanishcheva, I.; Sycheva, V.; Khasanova, N.; Antipov, E. Determination of lithium diffusion coefficient in LiFePO$_4$ electrode by galvanostatic and potentiostatic intermittent titration techniques. *Electrochim. Acta* **2010**, *55*, 2939–2950. [CrossRef]

24. Dees, D.W.; Kawauchi, S.; Abraham, D.P.; Prakash, J. Analysis of the Galvanostatic Intermittent Titration Technique (GITT) as applied to a lithium-ion porous electrode. *J. Power Sources* **2009**, *189*, 263–268. [CrossRef]

25. Tang, X.C.; Song, X.W.; Shen, P.Z.; Jia, D.Z. Capacity intermittent titration technique (CITT): A novel technique for determination of Li+ solid diffusion coefficient of LiMn$_3$O$_4$. *Electrochim. Acta* **2005**, *50*, 5581–5587. [CrossRef]

26. Kasper, M.; Leike, A.; Thielmann, J.; Winkler, C.; Al-Zubaidi R-Smith, N.; Kienberger, F. Electrochemical impedance spectroscopy error analysis and round robin on dummy cells and lithium-ion-batteries. *J. Power Sources* **2022**, *536*, 231407. [CrossRef]

27. Qu, D.; Malik, A.; Yu, H.C. Physics-based simulation of electrochemical impedance spectroscopy of complex electrode microstructures using smoothed boundary method. *Electrochim. Acta* **2022**, *432*, 141141. [CrossRef]

28. Nara, H.; Mukoyama, D.; Shimizu, R.; Momma, T.; Osaka, T. Systematic analysis of interfacial resistance between the cathode layer and the current collector in lithium-ion batteries by electrochemical impedance spectroscopy. *J. Power Sources* **2019**, *409*, 139–147. [CrossRef]

29. Gao, P.; Zhang, C.; Wen, G. Equivalent circuit model analysis on electrochemical impedance spectroscopy of lithium metal batteries. *J. Power Sources* **2015**, *294*, 67–74. [CrossRef]

30. Huang, J.; Li, Z.; Liaw, B.Y.; Zhang, J. Graphical analysis of electrochemical impedance spectroscopy data in Bode and Nyquist representations. *J. Power Sources* **2016**, *309*, 82–98. [CrossRef]

31. Wang, Y.; Gao, G.; Li, X.; Chen, Z. A fractional-order model-based state estimation approach for lithium-ion battery and ultra-capacitor hybrid power source system considering load trajectory. *J. Power Sources* **2020**, *449*, 227543. [CrossRef]

32. Sun, Y.; Li, Y.; Yu, M.; Zhou, Z.; Zhang, Q.; Duan, B.; Shang, Y.; Zhang, C. Variable fractional order - A comprehensive evaluation indicator of lithium-ion batteries. *J. Power Sources* **2020**, *448*, 227411. [CrossRef]

33. Zhu, G.; Kong, C.; Wang, J.V.; Kang, J.; Yang, G.; Wang, Q. A fractional-order model of lithium-ion battery considering polarization in electrolyte and thermal effect. *Electrochim. Acta* **2022**, 141461. [CrossRef]

34. Ruan, H.; Sun, B.; Jiang, J.; Zhang, W.; He, X.; Su, X.; Bian, J.; Gao, W. A modified-electrochemical impedance spectroscopy-based multi-time-scale fractional-order model for lithium-ion batteries. *Electrochim. Acta* **2021**, *394*, 139066. [CrossRef]

35. Yu, M.; Li, Y.; Podlubny, I.; Gong, F.; Sun, Y.; Zhang, Q.; Shang, Y.; Duan, B.; Zhang, C. Fractional-order modeling of lithium-ion batteries using additive noise assisted modeling and correlative information criterion. *J. Adv. Res.* **2020**, *25*, 49–56. [CrossRef]

36. Jia, Y.; Dong, L.; Yang, G.; Jin, F.; Lu, L.; Guo, D.; Ouyang, M. Parameter Identification Method for a Fractional-Order Model of Lithium-Ion Batteries Considering Electrolyte-Phase Diffusion. *Batteries* **2022**, *8*, 90. [CrossRef]

37. Zhang, L.; Wang, X.; Chen, M.; Yu, F.; Li, M. A fractional-order model of lithium-ion batteries and multi-domain parameter identification method. *J. Energy Storage* **2022**, *50*, 104595. [CrossRef]

38. Kumar, R.; Kant, R. Theory of quasi-reversible charge transfer admittance on finite self-affine fractal electrode. *Electrochim. Acta* **2011**, *56*, 7112–7123. [CrossRef]

39. Hirayama, M.; Sonoyama, N.; Abe, T.; Minoura, M.; Ito, M.; Mori, D.; Yamada, A.; Kanno, R.; Terashima, T.; Takano, M.; et al. Characterization of electrode/electrolyte interface for lithium batteries using in situ synchrotron X-ray reflectometry—A new experimental technique for LiCoO$_2$ model electrode. *J. Power Sources* **2007**, *168*, 493–500. [CrossRef]

40. Wei, S.; Li, Z.; Kimura, K.; Inoue, S.; Pandini, L.; Lecce], D.D.; Tominaga, Y.; Hassoun, J. Glyme-based electrolytes for lithium metal batteries using insertion electrodes: An electrochemical study. *Electrochim. Acta* **2019**, *306*, 85–95. [CrossRef]

41. Bai, L.; Xue, W.; Qin, H.; Li, Y.; Li, Y.; Sun, J. A novel dense LiCoO$_2$ microcrystalline buffer layer on a cathode-electrolyte interface for all-solid-state lithium batteries prepared by the magnetron sputtering method. *Electrochim. Acta* **2019**, *295*, 677–683. [CrossRef]

42. Lu, X.; Li, H.; Chen, N. An indicator for the electrode aging of lithium-ion batteries using a fractional variable order model. *Electrochim. Acta* **2019**, *299*, 378–387. [CrossRef]

43. Yang, C.; Song, J.; Wang, Y.; Wan, C. Impedance spectroscopic study for the initiation of passive film on carbon electrodes in lithium ion batteries. *J. Appl. Electrochem.* **2000**, *30*, 29–34. [CrossRef]

44. Davoodabadi, A.; Li, J.; Liang, Y.; Wood, D.L.; Singler, T.J.; Jin, C. Analysis of electrolyte imbibition through lithium-ion battery electrodes. *J. Power Sources* **2019**, *424*, 193–203. [CrossRef]

45. Westerlund, S.; Ekstam, L. Capacitor theory. *IEEE Trans. Dielectr. Electr. Insul.* **1994**, *1*, 826–839. [CrossRef]

46. Wang, B.; Li, S.E.; Peng, H.; Liu, Z. Fractional-order modeling and parameter identification for lithium-ion batteries. *J. Power Sources* **2015**, *293*, 151–161. [CrossRef]

47. Li, X.; Fan, G.; Pan, K.; Wei, G.; Zhu, C.; Rizzoni, G.; Canova, M. A physics-based fractional order model and state of energy estimation for lithium ion batteries. Part I: Model development and observability analysis. *J. Power Sources* **2017**, *367*, 187–201. [CrossRef]

48. Zou, C.; Zhang, L.; Hu, X.; Wang, Z.; Wik, T.; Pecht, M. A review of fractional-order techniques applied to lithium-ion batteries, lead-acid batteries, and supercapacitors. *J. Power Sources* **2018**, *390*, 286–296. [CrossRef]

49. Mu, H.; Xiong, R.; Zheng, H.; Chang, Y.; Chen, Z. A novel fractional order model based state-of-charge estimation method for lithium-ion battery. *Appl. Energy* **2017**, *207*, 384–393. [CrossRef]

50. Sabatier, J.; Merveillaut, M.; Francisco, J.M.; Guillemard, F.; Porcelatto, D. Lithium-ion batteries modeling involving fractional differentiation. *J. Power Sources* **2014**, *262*, 36–43. [CrossRef]

51. Alavi, S.; Birkl, C.; Howey, D. Time-domain fitting of battery electrochemical impedance models. *J. Power Sources* **2015**, *288*, 345–352. [CrossRef]

52. Unterrieder, C.; Zhang, C.; Lunglmayr, M.; Priewasser, R.; Marsili, S.; Huemer, M. Battery state-of-charge estimation using approximate least squares. *J. Power Sources* **2015**, *278*, 274–286. [CrossRef]

53. Duong, V.H.; Bastawrous, H.A.; Lim, K.; See, K.W.; Zhang, P.; Dou, S.X. Online state of charge and model parameters estimation of the LiFePO$_4$ battery in electric vehicles using multiple adaptive forgetting factors recursive least-squares. *J. Power Sources* **2015**, *296*, 215–224. [CrossRef]

54. Plett, G.L. Recursive approximate weighted total least squares estimation of battery cell total capacity. *J. Power Sources* **2011**, *196*, 2319–2331. [CrossRef]

55. Barré, A.; Deguilhem, B.; Grolleau, S.; Gérard, M.; Suard, F.; Riu, D. A review on lithium-ion battery ageing mechanisms and estimations for automotive applications. *J. Power Sources* **2013**, *241*, 680–689. [CrossRef]

56. Gao, Y.; Jiang, J.; Zhang, C.; Zhang, W.; Ma, Z.; Jiang, Y. Lithium-ion battery aging mechanisms and life model under different charging stresses. *J. Power Sources* **2017**, *356*, 103–114. [CrossRef]

57. Gao, Y.; Jiang, J.; Zhang, C.; Zhang, W.; Jiang, Y. Aging mechanisms under different state-of-charge ranges and the multi-indicators system of state-of-health for lithium-ion battery with Li(NiMnCo)O$_2$ cathode. *J. Power Sources* **2018**, *400*, 641–651. [CrossRef]

58. Lucu, M.; Martinez-Laserna, E.; Gandiaga, I.; Camblong, H. A critical review on self-adaptive Li-ion battery ageing models. *J. Power Sources* **2018**, *401*, 85–101. [CrossRef]

59. Han, X.; Ouyang, M.; Lu, L.; Li, J.; Zheng, Y.; Li, Z. A comparative study of commercial lithium ion battery cycle life in electrical vehicle: Aging mechanism identification. *J. Power Sources* **2014**, *251*, 38–54. [CrossRef]

60. Saha, B.; Goebel, K. *Battery Data Set*; NASA Ames Prognostics Data Repository, NASA Ames Research Center: Moffett Field, CA, USA, 2007.